Journal of Catalysis **195,** 326–335 (2000)
doi:10.1006/jcat.2000.3003, available online at http://www.idealibrary.com on IDEAL®

Structure–Activity Correlations for TON, FER, and MOR in the Hydroisomerization of *n*-Butane

Johannis A. Z. Pieterse,* K. Seshan,* and Johannes A. Lercher*,†,[1]

*Faculty of Chemical Technology, University of Twente, P.O. Box 217, 7500 AE, Enschede, The Netherlands; and †Institut für Technische Chemie, Technische Universität München, Lichtenbergstrasse 4, D-85748 Garching, Germany

Received March 5, 2000; revised July 6, 2000; accepted July 18, 2000

***n*-Butane hydroconversion was studied over (Pt-loaded) molecular sieves with TON, FER, and MOR morphology. The conversion occurs via a complex interplay of mono- and bimolecular bifunctional acid mechanism and monofunctional platinum-catalyzed hydrogenolysis. Hydroisomerization occurs bimolecularly at low temperatures. This is strongly indicated by the reaction order in *n*-butane of 2 for isobutane formation and the presence of 2,2,4-trimethylpentane among the products. Intracrystalline diffusion limitations of the reaction rates seem to be important for TON. Due to diffusion-controlled reaction rates for TON, the presence of Pt in TON was detrimental for the isomerization selectivity. As the ratio of utilized acid sites to accessible Pt becomes low (approximately 1 : 75), diffusion of the feed molecules to the acid sites is too slow to prevent Pt hydrogenolysis of *n*-butane. Reactions on H-FER occur predominantly on the outer surface and the pore mouth of the molecular sieve, presumably owing to rapid pore filling following a transient period of single-file diffusion. Due to high intrinsic activity toward (hydro)cracking this does not lead to high selectivity toward isobutane. Addition of Pt (bifunctionality) was in this case beneficial. Reaction at the external surface is not diffusion limited, allowing bifunctional nC_4 isomerization to occur. Although PtFER was found to approach selectivity levels as found for PtMOR, the latter has a significant advantage as the larger concentration of accessible acid sites leads to much higher activity.**

INTRODUCTION

Brønsted acidic H-mordenite as a component of commercial isomerization catalysts has received a lot of attention (1–8). *n*-Butane isomerization over mordenite was believed to occur via a bimolecular reaction pathway (involving dimerization, isomerization via methyl/hydride shifts, and cracking) (7, 8). Pt in mordenite has also been suggested to contribute to the isomerization of butane via a parallel bifunctional route involving dehydrogenation of the alkane on the metal site (5–7).

[1] To whom correspondence should be addressed. Fax: +49-89-28913544. E-mail: johannes.lercher@ch.tum.de.

It is interesting to rationalize the steric requirements for the bimolecular mechanism in the one-dimensional pores of mordenite. The kinetic diameters of branched alkanes (e.g., *i*-butane) approach the pore size of mordenite, implying that the individual molecules cannot pass each other within one channel. This type of motion is referred to as *single-file* diffusion (9). Generally, concentration gradients inside the pores are the driving force for the directed motion of the molecules. However, in single-file diffusion, a displaced molecule is more likely to return to its original position than to proceed further, since the latter would stipulate a further concentration of the molecules ahead (9), which seems to be highly constrained because of the space limitations in one-dimensional pores.

This becomes even more important when considering TON as a catalyst for *n*-butane isomerization. The pores of TON are straight unidirectional channels which have a significantly smaller diameter and coincide with the kinetic diameter of a singly branched alkane. In line with this, recent work by Martens *et al.* (10) describing the selective isomerization of long-chain alkanes over TON introduced the concept of shape-selective isomerization at crystal-terminating faces, termed pore mouth catalysis. Although there is solid kinetic evidence supporting this, several questions remain unanswered as already pointed out by Ernst (11). For instance, it is not clear whether the concept can be transferred to other reactants and other zeolite structures and what role the active sites at the external surface of the zeolite crystals play. In a recent paper (12) we showed that the acid sites in HFER and HTON are in principle sufficiently strong to polarize dibranched alkanes, but these sites are located in the pore mouth rather than fully at the external surface.

Intuitively, the concepts of pore mouth catalysis and single-file diffusion seem to be related as, at least for good back mixing, a concentration gradient across a zeolite particle does not exist. This situation then causes the reaction to be completely controlled by sites at the outer surface of the zeolites. For tubular flow reactors, a certain contribution of single-file diffusion related to the differential conversion

0021-9517/00 $35.00

may exist. However, a pure case of single-file diffusion is expected to occur only in membrane reactors.

The current contribution presents a kinetic study of *n*-butane conversion over zeolites with effectively unidirectional pores, i.e., TON, FER, and MOR under differential conditions and at low temperatures which favor a bimolecular reaction pathway. Unlike the higher linear analogues, the disfavored energetics for the formation of the primary carbenium ion intermediates favor *n*-butane (hydro)isomerization to occur via the bimolecular pathway demanding the formation of bulky branched C_8 intermediates. The choice of the zeolite, i.e., MOR, TON, and FER with different pore sizes, provides information on the ease of the bimolecular mechanism and how the steric constraints affect the place where the reaction takes place. The unidirectional MOR structure has cross sections with so-called side pockets allowing (small) molecules to pass each other. Next to its smaller pore size TON does not have this structural feature. FER has a two-dimensional structure with 10MR channels comparable to TON. The eight-membered apertures of FER are expected to exclude any contribution to the bimolecular reactions due to severe geometrical constraints (13, 14). However, the 8MR channels may ease the migration and accessibility of acid sites for *n*-butane.

METHODS

Catalysts

Na/K-FER and Na-MOR (obtained from TOSOH) with Si/Al ratios of 9 and 10, respectively, were used for the present investigation. Ion exchange of the samples in Na^+ form was performed with 1 M NH_4NO_3 (Merck Co., 101188.1000) at neutral pH and a temperature of 365 K, using approximately 7 ml of liquid per gram of solid. The procedure was repeated three times to ensure complete ion exchange. Finally, the sample was washed with distilled water. NH_4-TON was kindly donated by Exxon with a Si/Al ratio of 18 (TON-18) and by Shell (SRTCA), with Si/Al 20 (TON-20). From a solution of $Pt(NH_3)_4(OH)_2$, 0.1 wt% Pt was incorporated by ion exchange. The catalysts were calcined at 623 K (823 K for MOR) *ex situ* and reduced *in situ* at 623 K (823 K for MOR) for 1 h (MOR) and 2 h (TON and FER) in hydrogen flow (35 ml/min) before being used.

Characterization

The morphology and size of the crystallites were investigated by using a JEOL-JSM-35 CT scanning electron microscope. EDAX spectroscopy to determine total Si/Al ratios was performed on an S800 scanning electron microscope from Hitachi Co. equipped with a Kevex quantum detector energy dispersive X-ray system allowing elemental compositions to be determined within an accuracy of 5% (relative). The instrument had a resolution at 5.9 keV of 109 eV. In order to ensure that the data collected were representative of the whole sample, scans were made at more than one location. Calibration with a standard sample of known Si/Al ratio was performed prior to the measurements.

The NH_3 sorption measurements to determine acid site concentration and strength were performed on a modified Setaram TG-DSC 111 apparatus equipped with a Balzers QMS420 mass spectrometer to detect the concentration of desorbed substances from temperature-programmed desorption (see for more details Refs. 13, 15). The same system was used to record isotherms of nC_4 to explore the sorption capacity together with the heat of sorption.

FTIR measurements were performed with a Bruker IFS-88 spectrometer with a spectral resolution of 4 cm^{-1} and equipped with a Balzers QMS420 mass spectrometer, a vacuum cell, and a flow cell. The cells consisted of a stainless steal chamber equipped with CaF_2 windows and a resistance-heated furnace, in which a gold sample holder is placed. A self-supporting wafer was pressed and activated at 5 K/min to 823 K (673 K in the case of TON and FER) in either a stream of He or a base pressure of 10^{-7} mbar and the spectra were recorded with time resolution of approximately 30 s. A spectrum of the empty IR cell was used as reference (I_0) to convert the single-beam spectra (I) into absorbance spectra ($\log I_0/I$).

The Pt particle size was determined by using high-resolution transmission electron microscopy (HREM). A Philips CM 30 T electron microscope with a LaB_6 filament as the source of electrons was used, operated at 300 kV. Samples were mounted on a carbon polymer microgrid supported on a copper grid by placing a few droplets of a suspension of a ground sample in ethanol on the grid, followed by drying under ambient conditions.

Kinetic Experiments

The catalytic tests were performed in a fixed-bed tubular quartz reactor with an inner diameter of 5 mm and operated in continuous flow mode. For each test, 75 to 150 mg of catalyst was used. The catalyst was activated in flowing air (40 ml/min) at 5 K/min to 823 K in the case of MOR and 673 K in the case of FER and TON. In the case of Pt-containing catalysts, the stream of air was subsequently switched to a stream of 50 mol% hydrogen in helium for another hour. Finally, the catalysts were purged *in situ* at 673 K in flowing He. The reactor was then cooled to the reaction temperature, typically between 523 and 623 K. The reactant stream contained typically *n*-butane (Praxair, 99.95% purity, 0.02% iC_4 and 0.03% C_3 impurities), hydrogen, and helium. The reactor effluent was collected with an automatic sampling valve system, stored in multiloop valves, and subsequently analyzed by using a HP5890 gas chromatograph using a 50-m Al_2O_3/KCl capillary column equipped with a flame ionization detector and coupled to a mass-selective

detector, HP 5971A. The setup allowed for transient and steady-state experiments. Yields and selectivities were calculated on a carbon basis in mol% with corrections for the impurities in the feed. Kinetic analysis was carried out after 1 to 3 h of ageing after which no apparent changes in conversions could be observed. External mass-transfer limitation was checked for by changing the flow rate at constant space time and found to be absent under the present conditions.

RESULTS

Characterization

The physico-chemical properties of the materials are listed in Table 1. The dispersion of Pt decreased in the order PtMOR $\gg$ PtTON $\approx$ PtFER as deduced from TEM/EDX analysis. While for Pt–MOR Pt particle size was homogeneous below 0.5 nm, larger Pt particles were found in the case of Pt–TON and Pt-FER (0.5–3 nm). Therefore, considering the pore sizes, a significant fraction of Pt was located on the outer surface for FER and TON. Note, however, we cannot exclude the possibility of having Pt clusters below 0.5 nm also present inside the micropores (below the detection limit).

In the case of MOR, EDX analysis showed that Pt was distributed uniformly throughout the material. Ammonia calorimetry indicated that the strengths of the interaction with sorbed ammonia and the zeolite framework are very similar for all zeolites. This may indicate a similar acid strength assuming that the contribution of physisorption is similar for the zeolites. Gravimetric analysis of the adsorption of *n*-butane on the H form and Pt form of the zeolites showed that in the case of MOR the maximum loading at 13 mbar *n*-butane was the same for both cases. These observations indicate that the accessibility of the micropores in MOR did not change in the presence of platinum particles. A 10% lower sorption capacity for *n*-butane was evident in the case of PtTON compared to HTON, but not for PtFER. Note also, the numbers of acid sites gravimetrically determined with ammonia in the case of TON and FER were very similar irrespective of the presence of platinum (see Table 1).

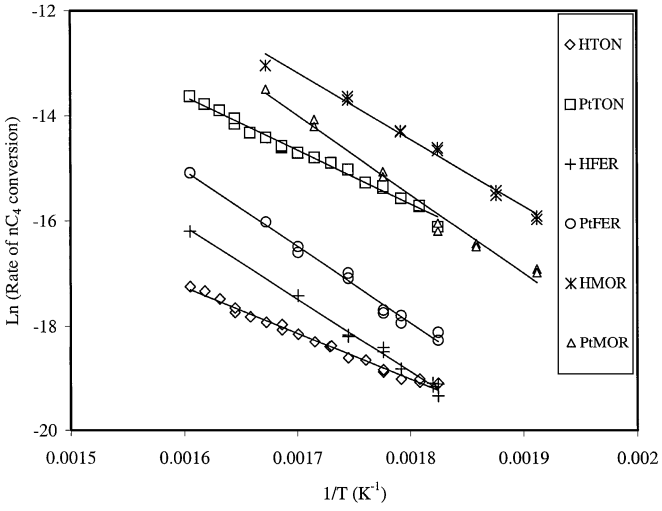

FIG. 1. Ln(rate of nC_4 conversion) as a function of $1/T$, $H_2/nC_4 = 4$, 280 mbar nC_4.

Kinetic Measurements

In the next paragraphs, the influences of various system variables are described.

Influence of temperature. All Pt-containing catalysts showed stable activity with time on stream. The H form of the zeolites showed stable activity with time on stream at temperatures below 573 K and typical conversion levels below 3%. At temperatures above 573 K, approximately 2 h time on stream was necessary to obtain stable catalyst operation. Figure 1 shows the (ln) rate of *n*-butane conversion as a function of the (inverted) temperature. In all cases, straight correlations could be obtained.

Figure 2 shows the influence of temperature on the product distributions obtained with HTON. The main products

TABLE 1

Physico-chemical Properties of the Materials

Catalyst	Si/Al total	Crystal size (001) (μm)	Acid sites (mmol/g)[a]	Brønsted acid sites (mmol/g)[b]	Lewis acid sites (mmol/g)[b]	ΔH NH_3 (kJ/mol)	ΔH nC_4 (kJ/mol)
HMOR	10	1.5	1.25	1.2	0.05	148	49
PtMOR	10	1.5	1.2	1.13	0.07	n.d.	48
HTON	20	2	0.49	0.43	0.07	140	59
HTON	18	4	0.65	0.50	0.15	n.d.	57
PtTON	18	4	0.63	0.57	0.06	n.d.	59.5
HFER	9	1.5	1.95	1.9	0.05	140	59
PtFER	9	1.5	1.90	n.d.	n.d.	n.d.	63.5

[a] Determined by ammonia sorption.
[b] Determined by ammonia and pyridine sorption.

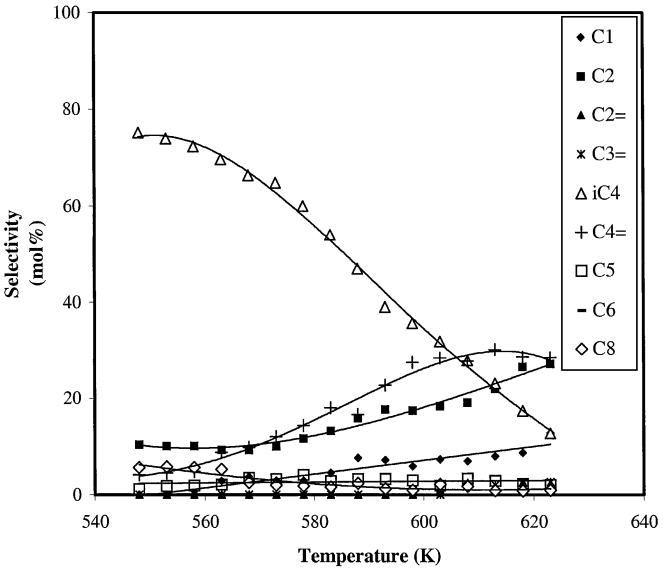

FIG. 2. Influence of temperature on the product distribution over HTON-18, $H_2/nC_4 = 4$, 280 mbar nC_4.

were methane, ethane, propane, isobutane, butenes, and pentanes. Also, a trace amount of 2,2,4-TMP was detected. Although the selectivity toward isomerization was rather high (about 75%) at 548 K, it decreased rapidly with temperature. Mainly methane, ethane, and propane (monomolecular cracking route) as well as butenes gained in importance with temperature at the cost of the selectivity to isomerization. Loading HTON-18 with 0.1 wt% Pt (at a hydrogen-to-*n*-butane ratio of 4) increased the formation of methane and ethane dramatically, which was attributed to metal (hydrogenolysis) activity (Fig. 3). Isomerization and disproportionation became less significant.

TABLE 2

Apparent Activation Energies (in kJ/mol) As Deduced from the Arrhenius Correlations between 523 and 623 K

	HTON $E_{act,app}$	PtTON $E_{act,app}$	HFER $E_{act,app}$	PtFER $E_{act,app}$	HMOR $E_{act,app}$	PtMOR $E_{act,app}$
Total	79 ± 2	86 ± 2	112 ± 5	118 ± 4	105 ± 4	120 ± 3
Methane	95	85	145	135	100	65
Ethane	118	81	120	125	105	75
Propane	119	84	130	131	135	143
i-Butane	53	130	111	112	100	135
Pentanes	63	115	—	—	115	150

In Table 2, the apparent activation energies are compiled for (Pt)TON. For HTON, very low activation energies for the formation of branched products (iC_4 and iC_5) were found. For PtTON, the activation energy (86.5 kJ/mol) compares well with the value found for *n*-hexane (hydro)conversion (16).

The main product found over HFER (Fig. 4) was ethane. Also, at temperatures above 560 K, C_1 and C_3 were abundant and in equimolar amounts indicating intrinsic activity for (hydro)cracking of feed butane. At lower temperatures, a clear excess of C_3 exists indicating an important additional (bimolecular) reaction route. Also, the level of unsaturated products appeared higher than in the case of HTON. iC_4 production was only marginal. Addition of Pt to HFER increased the selectivity toward iC_4 appreciably. With increasing the temperature, the selectivity slightly decreased mainly due to the increased metal activity (Fig. 5).

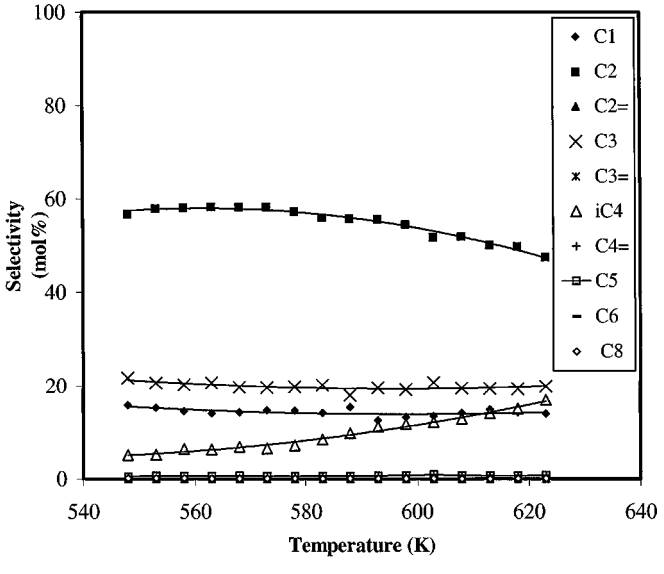

FIG. 3. Influence of temperature on the product distribution over PtTON-18, $H_2/nC_4 = 4$, 280 mbar nC_4.

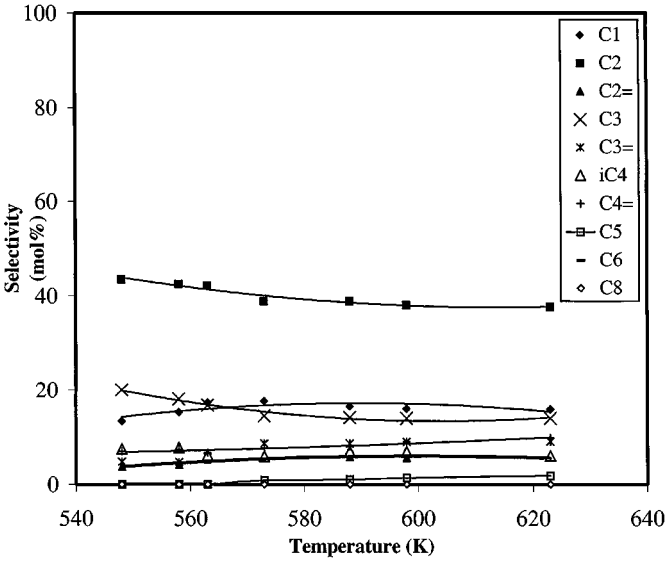

FIG. 4. Influence of temperature on the product distribution over HFER, $H_2/nC_4 = 4$, 280 mbar nC_4.

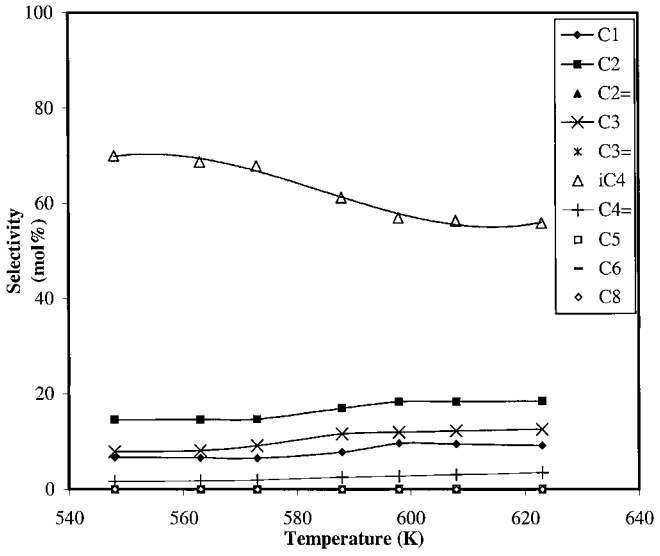

FIG. 5. Influence of temperature on the product distribution over PtFER, $H_2/nC_4 = 4$, 280 mbar nC_4.

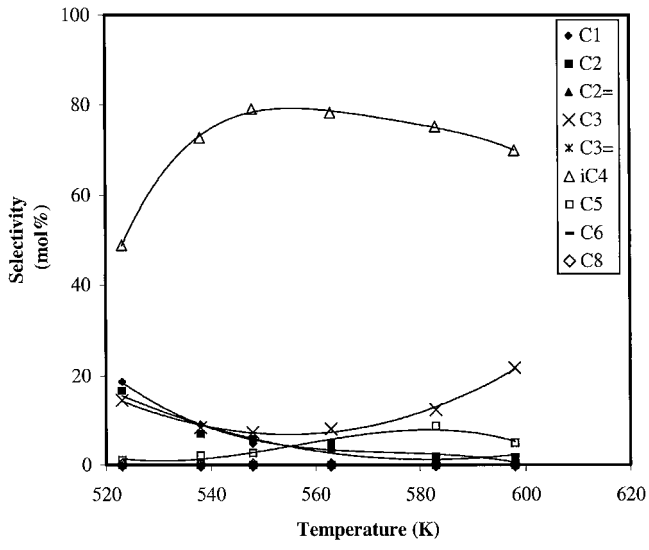

FIG. 7. Influence of temperature on the product distribution over PtMOR, $H_2/nC_4 = 4$, 280 mbar nC_4.

The activation energies for *n*-butane conversion were also higher than that found with TON. As in the case of TON, the presence of Pt in FER gave rise to slightly higher activation energy for *n*-butane conversion.

Product distributions found over mordenite are depicted in Figs. 6 and 7. The trends were in perfect agreement with those reported earlier (7). The isomerization selectivity for HMOR was the highest at lower temperatures (about 80%) but decreased significantly with increasing temperature. Unlike for HTON and HFER, where the cracking activity ($C_1 + C_3$) was remarkable, the loss in selectivity with temperature was mainly due to enhanced activity for disproportionation ($C_3 + C_5$). PtMOR shows the highest selectivity toward isomerization between 548 and 563 K. Below 548 K hydrocracking seemed to be an important side reaction, while at higher temperatures disproportionation gained importance at the expense of isomerization. As already seen for TON and FER, the activation energies for *n*-butane conversion were slightly higher in the presence of Pt.

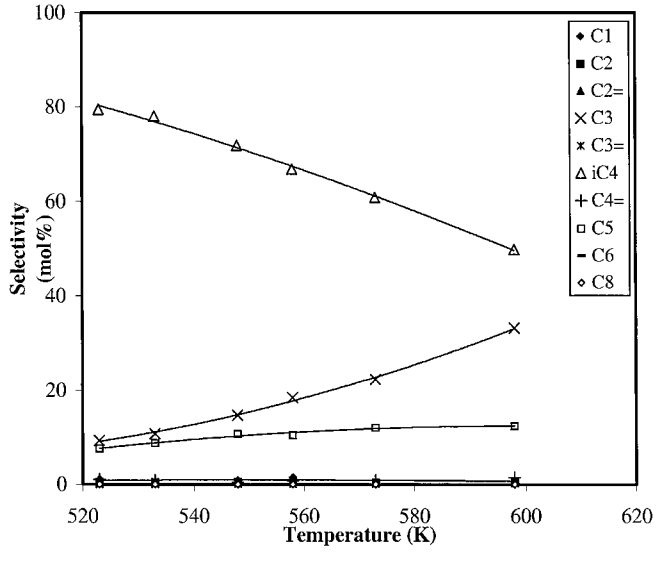

FIG. 6. Influence of temperature on the product distribution over HMOR, $H_2/nC_4 = 4$, 280 mbar nC_4.

Influence of variation of the space velocity. The WHSV was varied in order to vary the conversion. The main products formed (C_1–C_5) were concluded to be primary as indicated by the linear yield–conversion correlations.

The activities of the catalysts are compiled in Table 3 and the product distributions are compared in Table 4 at a total conversion of 0.9%. As described above, MOR was significantly more active than TON and FER. This cannot be explained on the basis of the acid site concentration. For MOR, it was argued that only one-third to two-thirds of the acid sites is accessible to alkanes without achieving a clear consensus (17–21). These accessible sites were suggested to

TABLE 3

TOF-based Activities for the Catalysts at 548 K and $H_2/nC_4 = 4$

Catalyst	TOF (h^{-1})
HTON	0.133
PtTON	1.525
HFER	0.065
PtFER	0.122
HMOR	6.9 (13.8)
PMOR	0.9 (1.8)

TABLE 4

Comparison of Selectivities (mol%) of Catalysts at 0.9% Conversion: $H_2/nC_4 = 4$, $P_{C_4} = 220$ mbar, $T = 548$ K

Catalyst	Methane	Ethane	Ethene	Propane	Propene	*i*-Butane	Butenes	Pentanes	Hexanes	2,2,4-TMP
HTON	0	12.6	0	3.8	0	72.8	4.1	1.2	0	5.5
PtTON	15.8	56	0	22	0	5.1	0	0.9	0	0.2
HFER	13.4	43.4	3.5	20	4.6	7.5	7	0.4	0	0.2
PtFER	6.7	13.7	0	7.8	0	70	1.6	0.2	0	0
HMOR	0.4	1	0.1	14.7	0.3	71.9	1.6	9.6	0.5	0
PtMOR	4	4.1	0	6.8	0	81	0.6	3.2	0.3	0

be located in the 12MR main channels. Our sorption studies show that the heat of sorption of nC_4 remains constant up to a coverage of at least 50% of the total amount of acid sites derived with ammonia sorption. Therefore, we conclude that at least 50% of the acid sites are accessible to *n*-butane. In this case, the TOF (see Table 3) of MOR exceeds the activity of TON and FER significantly, indicating that a much larger fraction of the acid sites of MOR was used for the reaction than with TON and FER (in Table 3 the TOF values calculated with 50% of the total concentration of acid sites are displayed in parentheses).

Influence of partial pressure n-butane. The logarithmic form of the power rate law

$$r = kp(nC_4H_{10})^m p(H_2)^n \qquad [1]$$

was used to compute the reaction orders in *n*-butane and product formation with *n*-butane pressure at hydrogen pressure of 730 mbar. The results are compiled in Table 5 with *n*-butane partial pressures varying between 280 and 100 mbar. The rates of *n*-butane conversion and product formation increased with *n*-butane partial pressure. This, however, becomes less significant at higher temperatures as shown here for TON. The same effect was reported earlier in the case of MOR (3). The orders are smaller in the case of Pt comprising zeolites than found for the H form parent materials. The reaction order in *n*-butane for the formation of isobutane as well as for the formation of pentanes was, as found before for MOR, close to 2 at 548 K. It was slightly lower at higher temperatures.

Influence of partial pressure hydrogen. The partial pressure hydrogen was varied between 180 and 800 mbar at a constant partial pressure *n*-butane of 200 mbar. The power rate law was applied to calculate the reaction orders in hydrogen (Eq. [1]). TON and FER show negative order in hydrogen with respect to the total conversion. The order becomes more negative when Pt is present. The same effect was found before for mordenite catalysts (3). Over HMOR, the selectivity to isobutane and isopentane increased slightly, while propane, ethane, and methane became less abundant with increasing hydrogen partial pressure. For PtMOR, increasing the partial pressure hydrogen decreased the isomerization activity at the benefit of mainly disproportionation and hydrogenolysis at 548 K. However, at higher temperatures the selectivity toward isomerization benefits from the increasing H_2/nC_4 ratio. A similar effect was found for PtTON. At 548 K the isomerization selectivity continued to decrease with increasing partial pressure hydrogen due to sigificant hydrogenolysis while at 598 K the selectivity increased until a H_2/nC_4 ratio of 1.9. A similar situation was found in the case of HTON at 598 K. In the case of PtFER at 598 K clearly a substantial increase in

TABLE 5

Orders (*n*) of the Reaction for *n*-Butane, Hydrogen, and Products

	HTON *n* (548 K, 573 K, 598 K)	PtTON *n* (573 K, 598 K)	HFER *n* (598 K)	PtFER *n* (598 K)	(Pt)HMOR[a] *n* (543 K, 573 K, 623 K)
Total	1.7, 0.9, 0.8	0.6, 0.3	0.8	1	1.5, 1, 0.5
Methane	0.3	0.5, 0.3	1	1.1	n.d.
Ethane	1, 0.6, 0.6	0.2, −0.3	1.1	1	n.d.
Propane	1.6, 1.5, 1.5	0.6, −0.2	2	1.1	n.d.
i-Butane	1.9, 1.9, 1.6	1.2, 1.1	2	1.2	1.3, 0.7, 0
Pentanes	2, 1.6, 1.6	1.6, 1.3	n.d.	n.d.	n.d.
2,2,4-TMP	−0.9, −1.2, −1.2	n.d.	−1.2	−0.9	n.d.
Hydrogen	−0.3	−0.5, −0.9	−0.3	−0.8	−0.2 (−0.4)[b]

[a] Taken from Ref. (3).
[b] Taken from Ref. (7). n.d., not determined.

hydrogenolysis with increasing partial pressure hydrogen was observed, diminishing the isomerization selectivity.

DISCUSSION

The conversion of *n*-butane over mordenite-based catalysts in the presence of hydrogen was investigated before at reaction temperatures between 523 and 623 K (7). Special attention was paid to the influence of Pt upon catalytic activity, selectivity, and stability. With H form mordenite the catalytic activity for *n*-butane conversion decreased markedly after a short time on stream. However, deactivation could be minimized by hydrogen in the presence of Pt. This was explained by a reduction of the concentration of intermediate olefins in the zeolite pores. The best results with respect to selective conversion of *n*-butane to isobutane were obtained for 0.05 to 0.25 wt% Pt on mordenite in the presence of hydrogen. Higher concentrations of Pt in the catalyst are shown to be detrimental for *n*-butane isomerization because of increasing selectivity to hydrogenolysis. *n*-Butane conversion was concluded to occur via a bimolecular mechanism involving a complex network of hydrogen transfer, oligomerization/cracking, isomerization, dehydrogenation, and hydrogenolysis (7).

On bifunctional catalysts three modes of alkane isomerization can (co)exist: monofunctional acid, monofunctional metallic, and bifunctional isomerization. These mechanisms are characterized by substantially different reaction kinetics and characteristic selectivities (24). The monofunctional acid mechanism via cyclopropyl carbenium ion (26) is characterized by a low activation energy (42–50 kJ/mol) and low reaction order in hydrogen (0) while the monofunctional metallic mechanism is distinguished by its high activation energy (230–293 kJ/mol) and highly negative reaction order in hydrogen (2–3.4). These values are related, however, to *n*-heptane, for which the isomerization on the acid sites does not occur via the much more demanding primary carbenium ion (which is claimed to have 100 kJ/mol higher true energy of activation (25)). The activation energies and reaction orders in hydrogen found for a bifunctional mechanism are reported to have values intermediate between those for the monofunctional catalysts. Typical values for $E_{act,app}$ for bifunctional isomerization of *n*-hexane (16) were 100–120 kJ/mol and orders between 1 and 0 for *n*-hexane conversion, and between −1 and 0 for the total order in hydrogen.

In the experiments, negative orders in hydrogen were found among all the samples indicating in all cases a significant contribution of the classical bifunctional mechanism. The reaction kinetics follow a negative order in hydrogen, because dehydrogenation–hydrogenation steps are equilibrated and the equilibrium concentrations of alkene intermediates decrease with increasing hydrogen pressure. The H form zeolites contained an iron impurity of about 0.02–0.04 wt% that can also have (de)hydrogenation functionality. However, Guisnet and co-workers pointed out that hydrogen may react with carbenium ions limiting their concentration (22). Over HMOR, hydrogen inhibited *n*-butane isomerization that occurs through a bimolecular pathway, but had practically no effect on *n*-hexane isomerization (monomolecular (16)). The bimolecular pathway requires the presence of neighboring alkoxide species, making this reaction more sensitive to concentration of alkoxide species on the surface. Indeed, the apparent activation energies for Pt comprising zeolites were in all cases higher than the value found for the H form of the zeolites. For Pt-containing zeolites also larger negative orders in hydrogen were found. Therefore, the higher $E_{act,app}$ is explained with Langmuir–Hinschelwood rate equations (assuming the surface reaction to be rate determining) that account for the inhibition of the reaction by hydrogen to some extent (23).

It is important to acknowledge that the values of E_{app} for *i*-butane formation found here (112–135) may not rule out a certain contribution of the monomolecular reaction pathway for isomerization of nC_4. Recent quantum chemical calculations point out that the activation energy for monomolecular isomerization of *n*-butene can proceed via an alkoxy intermediate (omitting the need for primary carbenium carbenium species) with an activation energy as low as 140 kJ/mol (25). Nevertheless, the presence of 2,2,4-trimethylpentane in the products and the positive order of about 2 for isobutane formation strongly favors, in general accordance with reaction conditions (high partial pressure and low temperatures), the bimolecular mechanism.

Brouwer (26, 27) proposed that trimethylpentane cations can rapidly equilibrate with all other trimethylpentane cations in liquid superacids, and the preferred cleavage pathway proceeds through the 2,2,4-trimethylpentane cation to form a tertiary isobutane cation and isobutene (isobutoxy goup). The formation of this species in the zeolite can be rationalized as follows: the C_8 intermediate that is initially formed from two *n*-butane surface species is most likely a secondary carbenium ion, i.e., 3,4-dimethylhexane, which can rapidly form a tertiary carbenium ion (2,4-dimethylhexane) via nonbranching methyl and hydride shifts. This species can undergo type B_1 cracking (for classification see Weitkamp (28)) to form a secondary *n*-butyl carbenium ion and an isobutyl species (see Fig. 8, route 1).

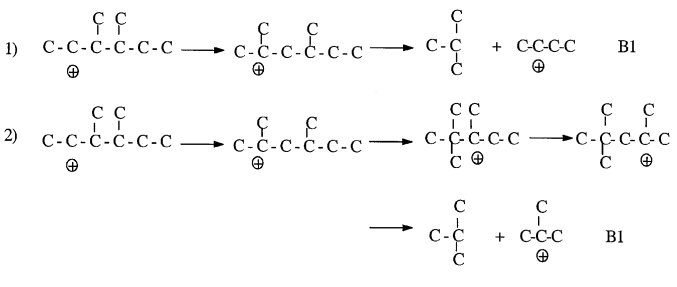

FIG. 8. Proposed mechanism for the formation of isobutane (26).

Alternatively, 2,4-dimethylhexane can form a secondary carbenium ion (2,2,3-trimethylpentane) via a branching rearrangement involving cyclopropyl ring formation and hydride shift. Subsequently, 2,2,3-trimethylpentane can form a tertiary carbenium ion, 2,2,4-trimethylpentane through nonbranching methyl and hydride shifts. Finally, 2,2,4-trimethylpentane cracks via the type B_1 (sec–tert) scission mechanism to yield isobutoxy and isobutyl species, eventually desorbing as isobutane via hydride transfer (see Fig. 8, route 2).

Type C cracking (sec–sec) of 2-methylheptane toward propane and pentene is suggested to cause part of the propane formed and pentane.

Another important route for the formation of propane in the case of HFER seems to be monomolecular cracking of feed butane to methane and propene, the latter being desorbed as propane due to fast hydride transfer. Lower apparent activation energies for the formation of C_1–C_3 over H form zeolites than found over Pt-comprising zeolites indicate that hydrogenolysis is of minor importance in comparison to the cracking mode in the case of the H form. However, this reaction route cannot satisfactorily explain the (still) nonstoichiometric formation of propane compared to that of methane.

A bimolecular reaction route is proposed to account for this, likely via the disproportionation of dimerized *n*-butane towards propane and *n*-pentane. Pentanes are, however, present only in trace amounts in the gas phase obtained with FER, which suggests their cracking toward ethane and propane. In accordance with such a proposal the excessive formation of propane compared to that of pentanes was reported previously in the literature for the conversion of *n*-butane over 12MR MOR and in particular for 10MR ZSM5 zeolites (7, 29). Guisnet and Gnep (29) reported that for HMFI, propane is formed in significant amounts, while practically no pentanes were observed. ^{13}C labeling experiments showed that this propane is formed via a bimolecular reaction pathway. The excessive propane formation was explained to be caused by limitations in desorption of branched products and steric constraints in the formation of the C_8 intermediates in the narrow pores of MFI (29). It can be suggested that a similar situation exists on comparing FER and TON (10MR like in the case of MFI) with 12 MR MOR, explaining excessive formation of propane over the 10MR zeolites in the present study.

The most likely bimolecular route for the formation of propane was independently reported by two groups to follow formation of C_9 alkoxy species, formed by the reaction between butene and C_5 alkoxy species (7, 29). C_9 alkoxy species undergo ß-scission forming hexene and propoxide species, the latter of which consume hydride from feed butane and desorb as propane. Additionally, hexene is protonated and undergoes cracking toward C_3 species that will again desorb as propane provided hydride transfer is sufficiently fast.

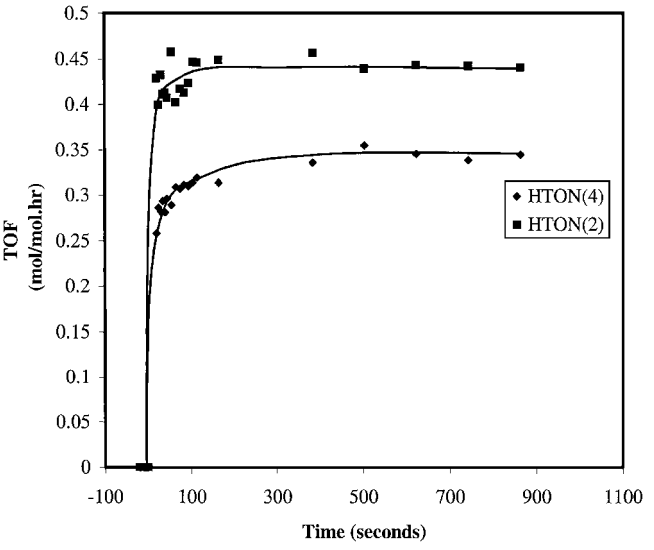

FIG. 9. Influence of crystal size on the activity over HTON, 220 mbar nC_4, $P_{tot} = 2$ bar.

The exceptionally low apparent activation energy for the formation of isobutane and isopentane for HTON-18 might be due to internal diffusion limitations. In order to investigate this, TON-18 was compared with TON-20. The samples had comparable acid site densities but different crystal sizes. The crystallite sizes in the 001 direction were 4 ± 1 and 2 ± 0.5 μm, respectively. The reaction was carried out without hydrogen in order to exclude a possible difference due to different negative orders in hydrogen. The smaller crystallites (TON-20, denoted as TON(2) in the legend of Fig. 9) showed on a TOF basis (normalized on the amount of Brønsted acid sites deduced from ammonia and pyridine sorption) about 1.5 times higher activity, supporting an internal diffusion-limited reaction sequence for HTON-18 (see Fig. 9). It is noteworthy that van der Runstraat *et al.* came to the same conclusion for hydroconversion of *n*-hexane over TON with crystallites sizing 4 μm (16). PtTON shows an $E_{act,app}$ of only 86.5 kJ/mol. This value matches well with the value found by van den Runstraat *et al.* for the hydroisomerization of *n*-hexane. As the $E_{act,app}$ for iC_4 and C_5 is 130 and 112 kJ/mol respectively, the low total activation energy for transformation of nC_4 is mainly caused by low $E_{act,app}$ for monomolecular cracking and hydrogenolysis. We conclude, therefore, that this catalyst does not comprise optimal bifunctionality following the Weisz intimacy criterium (32). The reaction of nC_4 on the Pt sites might cause the hydrogenation–dehydrogenation reaction to be not equilibrated. For PtTON, the much lower order for propane formation than for pentane formation indicates that propane is predominantly formed via hydrogenolysis and monomolecular cracking.

It was reported in the literature (30) that creating larger metal particles in MOR might locally destroy the zeolite,

creating three-dimensionality of the pore structure and, thus, increasing accessibility to acid sites. Especially in the case of TON and FER a good confinement of the Pt salt precursor might have implemented a local rupture of the micropore system by metallic Pt during reduction. Part of the enhanced total activity might in this situation be assigned to thus created higher accessibility of the acid sites. However, this is not directly supported by the nC_4 sorption studies, which show slightly less sorption capacity in the case of PtTON and no effect for FER. Also, the larger Pt particles are located on the outer surface as concluded from TEM analysis. Therefore, we do not believe that the accessibility of acid sites increased for the Pt-containing catalysts.

The decrease in the total order with increasing temperature and with the incorporation of Pt conceptually implies that the zeolite gets more covered. However, the temperature effect in the order of isobutane formation could also be reconciled by suggesting a change of the mechanism of isomerization from a bimolecular pathway at 548 K towards a more important role of the monomolecular pathway with increase of the temperature. The thermodynamics of the monomolecular pathway become more favorable at higher temperature. The presence of the monomolecular route has also been proposed by Tran *et al.* for nC_4 hydroisomerization over HMOR (31). However, lower reaction orders with increases of the temperature were also found for formation of pentanes, which can occur only via the bimolecular reaction route (see Table 5). Thus, the decrease in the order with temperature is due to the formation of more carbenium ions at the higher temperature.

Similarly, the decrease in the order of reaction in *n*-butane with the presence of Pt is explained by an enhanced formation of carbenium ions via butenes formed through dehydrogenation of *n*-butane on Pt. The same phenomenon can also explain the increase in the apparent activation energy (23). The increase of the coverage with temperature is interesting from the point of view of *single-file* diffusion. When the micropores are filled, a product molecule formed deep inside a pore cannot escape to the gas phase. In that case only sites near the pore mouths contribute to the conversion. This concept seems especially useful to explain the reactions over FER. HTON is found to be about 10 times less active than HMOR. Additionally, the TOF for HFER is about a factor of 2 lower than the one found with HTON. This suggests that HMOR utilizes much more acid sites than HTON which in turn utilizes more acid sites than HFER. In the case of FER, unlike for TON, indications for internal diffusion limitations could not be found. The $E_{act,app}$ is much higher than the one found for HTON and a deviation from linear for the Arrhenius plot was not observed. Therefore, the most plausible explanation for the trends found for FER is that reactions are restricted to the pore mouths. Owing to the high intrinsic cracking activity of HFER, this does not lead to high selectivity to isomerized products. The incorporation of Pt is in this case beneficial. Hydroconversion at the outer surface is not diffusion limited and transport of butene and/or isobutene between the Pt clusters located at the exterior and the adjacent pore mouths is fast enough to result in bifunctional catalysis at the outer surface. The suggestion that TON and especially FER utilize acid sites near the pore entrances is also supported by the presence of 2,2,4-trimethylpentane in the gas phase. The fact that this precursor for isobutane could never be observed in the case of MOR may find origin in the fact that this species inside the micropore structure will not be able to escape in the gas phase. However, the formation of this species at the pore mouth acid site allows desorption.

CONCLUSIONS

n-Butane hydroconversion was studied over (Pt-loaded) molecular sieves with TON, FER, and MOR morphology. The conversion occurs via a complex interplay of mono- and bimolecular bifunctional acid mechanism and monofunctional platinum-catalyzed hydrogenolysis. Hydroisomerization was concluded to occur (bifunctional) bimolecularly at low temperatures. This is evident from the reaction order in *n*-butane of 2 for isobutane formation and the presence of 2,2,4-trimethylpentane in the products. Intracrystalline diffusion limitations of the reaction rates seem to be important for TON. Due to diffusion-controlled reaction rates for TON, the presence of Pt in TON was detrimental for isomerization selectivity as diffusion of the feed molecules to the acid sites is too slow to prevent Pt from hydrogenolysis of *n*-butane. Reactions on HFER occur predominantly on the outer surface and the pore mouth of the molecular sieve, presumably owing to rapid pore filling following a single-file diffusion mechanism. Due to high intrinsic activity towards (hydro)cracking this does not lead to high selectivity toward isobutane. Addition of Pt (bifunctionality) was in this case beneficial. The reaction at the external surface is not diffusion limited, allowing bifunctional nC_4 isomerization to occur. Although PtFER was found to approach selectivity levels as found for PtMOR, the latter has a major advantage as the larger accessibility of acid sites leads to a much higher activity.

ACKNOWLEDGMENTS

Dr. M. J. G. Janssen (Exxon Chemical) is kindly acknowledged for donating the TON samples.

REFERENCES

1. Tonks, G. V., and Verstappen, A. E. L. M. M., U.S. Patent No. 5073667, 1991.
2. Mitsce, R. T., and Pollitzer, E. L., U.S. Patent No. 3544,451, 1970.

3. Asuquo, R. A., Eder-Mirth, G., and Lercher, J. A., *J. Catal.* **155**, 376 (1995).
4. Sie, S. T., *Stud. Surf. Sci. Catal.* **85**, 587 (1994).
5. Liu, H., Lei, G. D., and Sachtler, W. M. H., *Appl. Catal. A: General* **137**, 167 (1996).
6. Chao, K., Hung-Chung, W., and Leu, L., *J. Catal.* **157**, 289 (1995).
7. Asuquo, R. A., Eder-Mirth, G., Pieterse, J. A. Z., Seshan, K., and Lercher, J. A., *J. Catal.* **168**, 292 (1997).
8. Bearez, C., Chevalier, F., and Guisnet, M., *React. Kinet. Catal. Lett.* **22**, 405 (1983).
9. Kärger, J., Petzold, M., Pfeifer, H., Ernst, S., and Weitkamp, J., *J. Catal.* **136**, 283 (1992).
10. Martens, J. A., Souverijns, W., Verrelst, W., Parton, R., Froment, G. F., and Jacobs, P. A., *Angew. Chem., Int. Ed. Engl.* **107**, 2726 (1995).
11. Ernst, S., *Angew. Chem., Int. Ed. Engl.* **35**, 63 (1996).
12. Pieterse, J. A. Z., Veefkind-Reyes, S., Seshan, K., and Lercher, J. A., *J. Phys. Chem. B* **104**, 5715 (2000).
13. Eder, F., and Lercher, J. A., *J. Phys. Chem. B* **101**, 1273 (1997).
14. Van Well, W. J. M., Cottin, X., de Haan, J. W., van Hooff, J. H. C., Nivarthy, G., Lercher, J. A., Smit, B., and van Santen, R. A., *J. Phys. Chem.* **102**, 3945 (1998).
15. Eder, F., Stockenhuber, M., and Lercher, J. A., *Stud. Surf. Sci. Catal.* **97**, 495 (1995).
16. Van de Runstraat, A., Kamp, J. A., Stobbelaar, P. J., van Grondelle, J., Krijnen, S., and van Santen, R. A., *J. Catal.* **171**, 77 (1997).
17. Zholobenko, V. L., Makarova, M. A., and Dwyer, J., *J. Phys. Chem.* **97**, 5962 (1993).
18. Maache, M., Janin, A., Lavalley, J. C., and Benazzi, E., *Zeolites* **15**, 507 (1995).
19. Makarova, M. A., Wilson, A. E., van Liemt, B. J., Mesters, C. M. A. M., de Winter, A. W., and Williams, C., *J. Catal.* **172**, 170 (1997).
20. Datka, J., Gil, B., and Kubacka, A., *Zeolites* **17**, 428 (1996).
21. Eder, F., Stockenhuber, M., and Lercher, J. A., *Stud. Surf. Sci. Catal.* **97**, 495 (1995).
22. Tran, M.-T., Gnep, N. S., Guisnet, M., and Nascimento, O., *Catal. Lett.* **47**, 57 (1997).
23. Van Santen, R., *in* "Catalysis: An Integrated Approach to Homogeneous, Heterogeneous and Industrial Catalysis" (J. A. Moulijn, P. W. N. M. van Leeuwen, and R. A. Van Santen, Eds.). Elsevier, Amsterdam, 1993.
24. Belloum, M., Travers, Ch., and Bournonville, J. P., *Rev. Inst. Français Pétrole* **46**, 89 (1991).
25. Corma, A., *J. Phys. Chem. A* **102**, 982 (1998).
26. Brouwer, D. M., and Hogeveen, H., *Prog. Phys. Org. Chem.* **9**, 192 (1972).
27. Brouwer, D. M., *in* "Chemistry and chemical engineering of catalytic processes" (R. Prins and G. C. A. Schuit, Eds.), Vol. 137. Sijthoff & Noordhof, Alphen a/d Rijn, 1980.
28. Weitkamp, J., *Appl. Catal.* **8**, 123 (1983).
29. Guisnet, M., and Gnep, N. S., *Appl. Catal. A: General* **146**, 33 (1996).
30. Carvill, B. T., Lerner, B. A., Adelman, B. J., Tomczak, D. C., and Sachtler, W. M. H., *J. Catal.* **144**, 1 (1994).
31. Tran, M.-T., Gnep, N. S., Szabo, G., and Guisnet, M., *J. Catal.* **174**, 185 (1998).
32. Weisz, P. B., *in* "Advances in Catalysis and Related Subjects, Vol. 13" (D. D. Eley, P. W. Selwood, and P. B. Weisz, Eds.), p. 157. Academic Press, London, 1963.